

Rare-event statistics of subthreshold self-focusing

A. M. Zheltikov

Institute of Quantum Science and Engineering, Department of Physics and Astronomy, Texas A&M University, College Station, Texas 77843, USA

(Received 4 September 2023; revised 10 November 2023; accepted 21 November 2023; published 26 January 2024)

Canonical nonlinear optics treats self-focusing as a deterministic beam evolution scenario, unfolding above the self-focusing threshold due to the intensity-dependent change in the refractive index. While this deterministic view is adequate for a vast class of nonlinear processes, its insight into stochastic nonlinear phenomena, including laser-induced damage and self-focusing-enhanced spectral transformations, is limited. Here, we present a stochastic treatment of self-focusing. We derive a closed-form analytical solution for the count rate of extreme self-focusing events in nonlinear beam dynamics below the self-focusing threshold. We show that the rare-event statistics of subthreshold self-focusing is highly sensitive to the signal-to-noise ratio and the bandwidth of the laser field waveform. For low-signal-to-noise beams, the rare-event distribution of deeply subthreshold self-focusing is shown to exhibit a manifestly nonexponential tail, thus indicating the enhancement of extreme self-focusing events. We show that subthreshold self-focusing is further enhanced by a broader bandwidth of the noise component of the laser field. It is such broadband, low-signal-to-noise laser fields that are especially prone to deeply subthreshold, rogue-wave self-focusing, lowering, via a laser-induced breakdown, the lifetime of downstream optics.

DOI: [10.1103/PhysRevA.109.013520](https://doi.org/10.1103/PhysRevA.109.013520)**I. INTRODUCTION: DETERMINISTIC VIEW OF SELF-FOCUSING**

Self-focusing is one of the central effects in nonlinear optics [1–3]. Its discovery [4,5] is among the most significant milestones of nonlinear-optical physics. Self-focusing plays a central role in ultrafast laser technologies as it provides a mechanism whereby the lasing modes can be locked to enable stable ultrashort light pulse generation [6,7]. In a vast variety of light-matter interaction scenarios, however, self-focusing is an inevitable and uncontrollable companion of nonlinear spectral and temporal transformations of optical field waveforms, enhancing nonlinear processes and making interpretation of experiments difficult [1–3]. In some of more interesting settings, self-focusing acts in concert with other nonlinear processes, giving rise to laser filamentation [8–10], remarkably efficient supercontinuum generation [11,12], and cross-range wavelength conversion [13]. Typical of high-power lasers is the manifestation of self-focusing as a primary cause of damage to optical components, which sets a limit on the peak power of the laser output. It is this act of self-focusing that the celebrated technology of chirped-pulse amplification [14] is targeted at and helps to avoid as a route toward higher-energy and higher-intensity laser pulses [15].

Paralleling its centrality to the experimental scenery of optical physics and laser technologies, the theory of self-focusing [1–3] has a very special place in conceptual foundations of nonlinear wave dynamics. Not only does this theory help understand self-focusing and its manifestations in laser-matter interactions, but it also reveals the Hamiltonian structure of the underlying beam dynamics and sets a framework for the analysis of a vast class of nonlinear wave phenomena in electrodynamics, plasma physics,

oceanography, and quantum science. Inherent in this framework is the view of beam self-focusing as a part of deterministic field-waveform dynamics. As a hallmark result of this theory, a laser beam with a peak power P above the critical power of self-focusing, P_s , undergoes self-focusing as a whole due to the transverse profile of the intensity-dependent refractive index [1,2]. In its most general form, the critical power of self-focusing can be written as [16] $P_s = \alpha(4\pi n_0 n_2)^{-1} \lambda^2$, where n_0 is the field-free refractive index, n_2 is the nonlinear refractive index, λ is the laser wavelength, and α is a constant that is independent of the material properties, but depends on the beam profile and boundary conditions. Specifically, the canonical textbook by Boyd [17] suggests $\alpha \approx (0.61\pi)^2/2 \approx 1.83$ for a generic Gaussian-beam self-focusing geometry.

In addition to beam self-focusing as a whole, high-intensity laser fields are prone to small-scale self-focusing, induced by spatial modulation instabilities (MIs) [18], which tend to build up across a laser beam within a propagation path on the order of the nonlinear length, $l_{nl} \sim \lambda/(2\pi n_2 I)$, where $I = I(\mathbf{r}, t)$ is the laser field intensity, \mathbf{r} is the position vector, and t is the time. Thus, given a nonlinear medium of length L , the threshold of MI-induced small-scale self-focusing can be defined, in agreement with the available analytical solutions [19–22], numerical simulations [23], and experimental results [24], as

$$I_0 \sim \lambda/(2\pi n_2 L). \quad (1)$$

For laser pulses with $I > I_0$, spatial MIs give rise to field-intensity hot spots across the laser beam [25,26], leading to beam breakup into filaments with a typical radius r_f , such that the peak power within a filament is, roughly, the critical power of self-focusing, $\pi r_f^2 I \sim P_s$. In solid-state materials,

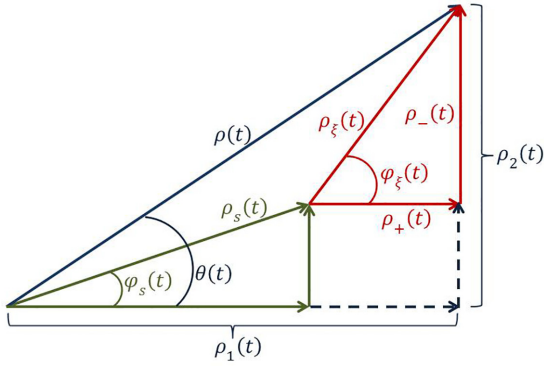


FIG. 1. An Argand diagram of the stochastic field waveform $\eta(t)$ as defined by Eqs. (2) and (3) (blue arrow) along with its deterministic component $s(t)$ (green arrow) and random part $\xi(t)$ (red line). Also shown are the phase $\theta(t)$ of the field waveform $\eta(t)$ (blue), the phase $\varphi_s(t)$ of the deterministic field $s(t)$ (green), and the noise $\xi(t)$ (red), as well as the $\rho_1(t)$ and $\rho_2(t)$ components of $\eta(t)$ and the $\rho_+(t)$ and $\rho_-(t)$ components of the noise.

enhanced photoionization in field hot spots inherent in such beam dynamics leads to optical damage [27,28].

While this view of self-focusing is fully adequate for a vast class of nonlinear wave phenomena [1–3,17], its insight into the stochastic aspects of nonlinear beam dynamics is limited. As most prominent examples, laser-induced damage, as well as self-focusing-enhanced stimulated-scattering and frequency-conversion effects are notoriously difficult to understand and quantify in terms of the deterministic approach as the detectable signatures of such processes are manifestly probabilistic in their nature, evading categorization in deterministic terms. Here, we focus on probabilistic aspects of self-focusing, paying special attention to extreme self-focusing events in nonlinear beam dynamics of a noisy laser field well below the self-focusing threshold. We will derive a closed-form analytical solution for the count rate of extreme self-focusing events in nonlinear beam dynamics of noisy laser fields deeply below the self-focusing threshold. Analysis of this solution shows that the rare-event statistics of such deeply subthreshold self-focusing is highly sensitive to the signal-to-noise ratio and the bandwidth of the laser field waveform.

II. STOCHASTIC MODEL OF A DRIVER

Central to our stochastic analysis of self-focusing is the treatment of the field waveform, $\eta(t)$, as a random process and a search for the probability distribution of the number of excursions of this random process across the level set by the self-focusing threshold. To proceed with this program, we consider a generic stochastic field waveform $\eta(t)$ [Figs. 1 and 2(a)–2(d)], represented as a superposition

$$\eta(t) = s(t) + \xi(t) \quad (2)$$

of a deterministic waveform $s(t) = \rho_s(t)\cos[\omega_0 t + \varphi_s(t)]$ [Figs. 1 and 2(a)] and a narrowband noise $\xi(t) = \rho_\xi(t)\cos[\omega_0 t + \varphi_\xi(t)]$ [Figs. 1 and 2(b)].

Central to the canonical framework of nonlinear optics is the description of light-matter interactions in terms of

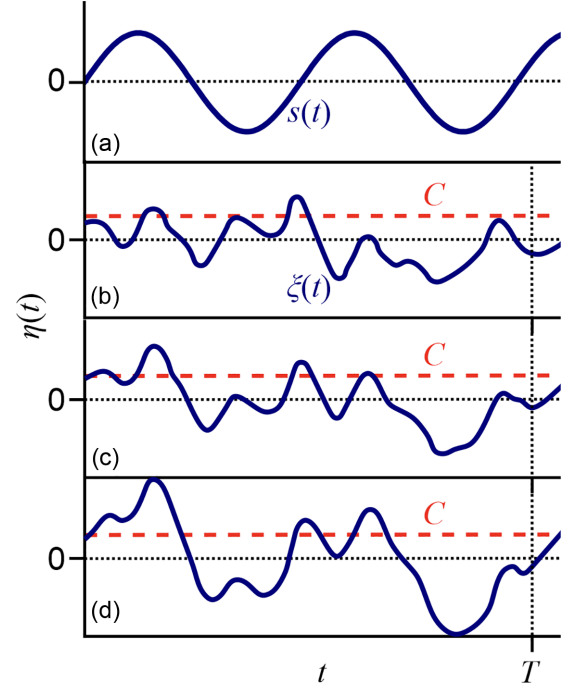


FIG. 2. A random process representing the driver waveform $\eta(t)$ [Eq. (1)]: (a) the regular, deterministic component $s(t)$; (b)–(d) the waveform $\eta(t) = s(t) + \xi(t)$ with the signal-to-noise ratio $a = 0$, (b)–(d). With $a = 0$, $\eta(t) = \xi(t)$. Also shown are the threshold C (red dashed line) and the detection time T (vertical dotted line).

nonlinear evolution equations for the field envelopes with a nonlinear source term expressed via a suitable nonlinear polarization [1,17,29]. The nonlinear polarization, in its turn, is expressed in this framework as a product of pertinent field envelopes. Such a framework has been proven adequate for a remarkably broad variety of nonlinear-optical processes, including, but not limited to self-focusing, self- and cross-phase modulation, parametric amplification, wave mixing, and low-order harmonic generation [1,17,29]. Specifically, providing a kernel for the Kerr nonlinearity, leading to self-focusing and self-phase modulation, is the nonlinear change in the refractive index, $\Delta n(\mathbf{r}, t) = n_2 I(\mathbf{r}, t)$, where the intensity $I(\mathbf{r}, t)$ is defined as a quadratic form of the field envelope [1,17]. Nonlinear processes sensitive to the field carrier, such as photoionization-induced absorption and refraction, can be included into this framework [8,9,30], e.g., via suitably defined photoionization currents [9,31]. Such processes fall beyond the scope of this study.

To extend this standard treatment of nonlinear optics to stochastic field waveforms, we seek to isolate the envelope of the field waveform (1). To this end, we rewrite $\eta(t)$ as [32,33]

$$\eta(t) = \rho(t)\cos[\omega_0 t + \theta(t)], \quad (3)$$

where $\rho(t) = \{[\rho_1(t)]^2 + [\rho_2(t)]^2\}^{1/2}$, $\theta(t) = \text{atan}[\rho_2(t)/\rho_1(t)]$, $\rho_1(t) = \rho_s(t)\cos[\varphi_s(t)] + \rho_+(t)$, $\rho_2(t) = \rho_s(t)\sin[\varphi_s(t)] + \rho_-(t)$, $\rho_+(t) = \rho_\xi(t)\cos[\varphi_\xi(t)]$, and $\rho_-(t) = \rho_\xi(t)\sin[\varphi_\xi(t)]$. An Argand diagram of the stochastic field waveform $\eta(t)$ as defined by Eqs. (2) and (3) is presented in Fig. 1, which shows the envelopes $\rho_s(t)$, $\rho_\xi(t)$, and $\rho(t)$ and the respective phases $\varphi_s(t)$, $\varphi_\xi(t)$, and $\theta(t)$, as well as the $\rho_1(t)$ and $\rho_2(t)$

components of $\eta(t)$ and the $\rho_+(t)$ and $\rho_-(t)$ components of the noise.

We set $\xi(t)$ to be a normally distributed stationary random process with a variance σ^2 and symmetric spectral density $S(\omega)$, such that Ω for any Ω , and correlation function

$$R(\tau) = \pi^{-1} \int_{-\infty}^{\infty} S(\omega_0 - \Omega) \cos \Omega \tau d\Omega. \quad (4)$$

The joint distribution of $\rho_1(t)$ and $\rho_2(t)$ is then given by

$$w_2(\rho_1, \rho_2) = (2\pi)^{-1} \sigma^{-2} \exp[-(\rho_+^2 + \rho_-^2)/(2\sigma^2)].$$

The joint distribution of the envelope ρ and phase θ can now be found as

$$w_2(\rho, \theta) = |\partial(\rho_1, \rho_2)/\partial(\rho, \theta)| w_2(\rho_+ = \rho \cos \theta - \rho_s \cos \varphi_s, \rho_- = \rho \sin \theta - \rho_s \sin \varphi_s),$$

leading to [33]

$$w_2(\rho, \theta) = \rho/(2\pi\sigma^2) \exp \left\{ - \left[(\rho^2 - 2\rho_s \rho \cos(\theta - \varphi_s) + \rho_s^2)/(2\sigma^2) \right] \right\}, \quad (5)$$

Integrating this distribution in θ , we find the envelope distribution:

$$W_\rho(\rho) = (\rho/\sigma^2) \exp[-(\rho^2 + \rho_s^2)/(2\sigma^2)] I_0(\rho\rho_s/\sigma^2), \quad (6)$$

where $I_0(x)$ is the modified Bessel function of the first kind.

The probability density of the normalized envelope $v = \rho/\sigma$ is

$$W_v(v) = \mathcal{Q}(v, a) = v \exp[-(a^2 + v^2)/2] I_0(av), \quad (7)$$

where $a = \rho_s/\sigma$ is recognized as the signal-to-noise ratio, and $\mathcal{Q}(v, a)$ is often referred to as the Rice distribution [34,35].

The envelope $\rho_s(t)$ of the regular signal $s(t)$ in our model of the stochastic driver [Eq. (3)] is a slowly varying function of time. The timescale of its variations, $\tau_\rho = \rho_{s0} |d\rho_s(t)/dt|^{-1}$, is much larger than the timescale fluctuations of $\xi(t)$. On a timescale shorter than τ_ρ , $a(t) = \rho_s(t)/\sigma$ is thus a meaningful measure of the signal-to-noise ratio. Specifically, with t chosen close to t_0 such that $\rho_s(t_0) = \rho_{s0} = \max_t \{\rho_s(t)\}$, the ratio $a = \rho_s(t)/\sigma = \rho_{s0}/\sigma$ characterizes the signal-to-noise ratio near the peak of the driver pulse. With this picture in mind, we will follow the tradition [33] and omit the time argument of $a(t)$ hereinafter, operating on the understanding that this parameter generally varies from the peak of the pulse to its edges.

Integrating the joint distribution $w_2(\rho, \theta)$ in Eq. (5) in ρ , we find for the distribution of the phase θ

$$W_\theta(\theta) = (2\pi)^{-1} \exp(-a^2/2) \{1 + (\pi)^{1/2} \chi \times \exp(\chi^2) [1 + \Phi(\chi)]\}, \quad (8)$$

where $\chi = (2)^{-1/2} a \cos(\theta - \varphi_s)$ and $\Phi(\chi) = 2(\pi)^{-1/2} \int_0^\chi \exp(-u^2) du$.

When $a = 0$, i.e., the deterministic part of the field is zero, $\rho_s = 0$, Eq. (7) reduces to the Rayleigh distribution $\mathcal{R}(v)$,

$$W_\rho(v) = \mathcal{Q}(v, 0) = \mathcal{R}(v) = v \exp(-v^2/2). \quad (9)$$

The phase θ is then uniformly distributed within 2π , $W_\theta(\theta) = (2\pi)^{-1}$.

In the opposite limit of $a \gg 1$, both $W_\rho(\rho)$ and $W_\theta(\theta)$ become Gaussian:

$$W_\rho(\rho) = (2\pi)^{-1/2} \sigma^{-1} \exp[-(\rho - \rho_s)^2/(2\sigma^2)], \quad (10)$$

$$W_\theta(\theta) = (2\pi)^{-1/2} a \exp[-a^2(\theta - \varphi_s)^2/2]. \quad (11)$$

As $a \rightarrow \infty$, the stochastic character of the envelope and phase is totally suppressed, as their distributions tend to delta functions centered, respectively, at ρ_s and φ_s , $W_\rho(\rho) \rightarrow \delta(\rho - \rho_s)$ and $W_\theta(\theta) \rightarrow \delta(\theta - \varphi_s)$.

III. THRESHOLD-CROSSING STATISTICS

As $\eta(t)$ fluctuates as a function of time, its envelope $\rho(t)$ may cross a preset level $C = C_\rho$ (red dashed line in Fig. 2), making excursions into the area above C_ρ , in the course of these fluctuations. For each realization of $\eta(t)$, the number $n(C_\rho, T)$ of such crossings within a time interval from t_0 to $t_0 + T$ is a random function of C_ρ and T , $n(C_\rho, T) = n^+(C_\rho, T) + n^-(C_\rho, T)$, where $n^+(C_\rho, T)$ and $n^-(C_\rho, T)$ are the numbers of upward and downward crossings, i.e., crossings with positive and negative slopes of $\rho(t)$ [Figs. 2(b)–2(d)].

The mean number $N_\rho^+(C_\rho, T) = \langle n^+(C_\rho, T) \rangle$ of upward crossings is given by [36–38]

$$N_\rho^+(C_\rho, T) = \int_{t_0}^{t_0+T} dt \int_0^\infty \dot{\rho} w_{\rho 2}(C_\rho, \dot{\rho}) d\dot{\rho}, \quad (12)$$

where $w_{\rho 2}(\rho, \dot{\rho})$ is the joint probability density of ρ and its time derivative $\dot{\rho}$.

Provided that $\eta(t)$ is stationary, the outer integral in Eq. (12) is reduced to a multiplication by T , leading to the following result for the rate of positive-slope crossings between $\rho(t)$ and C_ρ :

$$v_\rho(C_\rho) = T^{-1} N_\rho^+(C_\rho, T) = \int_0^\infty \dot{\rho} w_{\rho 2}(C_\rho, \dot{\rho}) d\dot{\rho}. \quad (13)$$

To find the joint probability density of the envelope and its derivative for $\eta(t)$ as defined by Eqs. (2) and (3), we consider six random variables: $x_1 = \rho_+$, $x_2 = \dot{\rho}_+$, $x_3 = \ddot{\rho}_+$, $x_4 = \rho_-$, $x_5 = \dot{\rho}_-$, and $x_6 = \ddot{\rho}_-$. The envelope ρ is not normally distributed [Eqs. (6) and (7)], but $x_1, x_2, x_3, x_4, x_5, x_6$ are. The joint probability distribution for n normal random variables ξ_i with variances σ_i , $i = 1, 2, \dots, n$, is generally found as

$$w_n(\xi_1, \xi_2, \dots, \xi_n) = (2\pi)^{-n/2} D^{-1/2} \sigma_1^{-1} \sigma_2^{-1} \dots \sigma_n^{-1} \times \exp \left[-(2D)^{-1} \sum_{i,j=1}^n D_{ij} \sigma_i^{-1} \sigma_j^{-1} (\xi_i - \langle \xi_i \rangle) (\xi_j - \langle \xi_j \rangle) \right] \quad (14)$$

where D is the determinant:

$$D = \begin{vmatrix} 1 & r_{12} & \dots & r_{1n} \\ r_{21} & 1 & \dots & r_{2n} \\ \dots & \dots & \dots & \dots \\ r_{n1} & r_{n2} & \dots & 1 \end{vmatrix},$$

$r_{ij} = \sigma_i^{-1} \sigma_j^{-1} \langle (\xi_i - \langle \xi_i \rangle) (\xi_j - \langle \xi_j \rangle) \rangle$, and D_{ij} is the cofactor of r_{ij} .

The variances of x_i , $i = 1, \dots, 6$, are $\sigma_1^2 = \sigma_4^2 = \sigma^2$, $\sigma_2^2 = \sigma_5^2 = -\sigma^2 R_0''$, and $\sigma_3^2 = \sigma_6^2 = \sigma^2 R_0^{(4)}$, where $R_0'' = [d^2 R(\tau)/d\tau^2]_{\tau=0}$ and $R_0^{(4)} = [d^4 R(\tau)/d\tau^4]_{\tau=0}$. The determinant D in Eq. (14) is $D = \{[R_0^{(4)} - (R_0'')^2]/R_0^{(4)}\}^2$.

Applying Eq. (14) to find $w_6(x_1, x_2, x_3, x_4, x_5, x_6)$, transforming the result to $W_6(\rho, \dot{\rho}, \ddot{\rho}, \theta, \dot{\theta}, \ddot{\theta})$ and integrating it in $\theta, \dot{\theta}, \ddot{\theta}, \dot{\rho}$, we find

$$w_{v2}(v, \dot{v}) = v/(2\pi\varepsilon) \exp[-(a^2 + v^2 - \dot{v}^2/R_0'')/2] I_0(av) \quad (15)$$

where $\varepsilon = [|R_0''|/(2\pi)]^{1/2}$.

Plugging Eq. (15) into Eq. (13) and performing a straightforward integration in $\dot{\rho}$, we find

$$v_\rho(C_\rho) = \varepsilon(C_\rho/\sigma) \exp[-(a^2 + C_\rho^2/\sigma^2)/2] I_0(aC_\rho/\sigma). \quad (16)$$

When $a = 0$, i.e., the deterministic part of the field is zero, Eq. (16) reduces to

$$v_{\rho0}(C_\rho) = \varepsilon \mathcal{R}(C_\rho) = \varepsilon(C_\rho/\sigma) \exp[-C_\rho^2/(2\sigma^2)]. \quad (17)$$

As one of its significant properties, the solution (16) for $v_\rho(C_\rho)$ is seen to factorize as

$$v_\rho(C_\rho) = \varepsilon W_\rho(C_\rho/\sigma) = \varepsilon \mathcal{Q}(C_\rho/\sigma, a), \quad (18)$$

where $W_\rho(x)$ is as defined by Eq. (6).

Solution (16) is known from the earlier studies of the level-crossing properties of random processes [38–40] and proven useful for the analysis of multipath radio-signal propagation [41]. In this study, we bring this solution into a context of nonlinear optics, resorting to Eq. (16) as the first step in a stochastic treatment of self-focusing.

IV. THE COUNT RATE OF SELF-FOCUSING EVENTS

While it offers much-needed resources for our analysis, Eq. (16) is not yet the solution needed to describe the rare-event statistics of $I < I_{\text{MI}}$ self-focusing. Indeed, as an expression of nonlinearity of underlying wave dynamics, the MI threshold I_{MI} [Eq. (1)] is defined with respect to a nonlinear function of the driver envelope, $\psi(t) = f([\rho(t)])$, rather than the driver envelope itself. The rare-event statistics of such nonlinear dynamics thus connects to the mean number of upward crossings $N_\psi^+(C_\psi, T)$ between $\psi(t)$ and $C_\psi = f(C_\rho) = C_\rho^2/2$ within a time interval from t_0 to $t_0 + T$,

$$N_\psi^+(C_\psi, T) = \int_{t_0}^{t_0+T} dt \int_0^\infty \dot{\psi} w_{\psi2}(C_\psi, \dot{\psi}) d\dot{\psi}, \quad (19)$$

where $w_{\psi2}(\psi, \dot{\psi})$ is the joint probability density of ψ and its time derivative $\dot{\psi}$ and $w_{\psi2}(C_\psi, \dot{\psi})$ is obtained from $w_{\psi2}(\psi, \dot{\psi})$ by formally replacing $x_1 = \psi$ by $x_1 = C_\psi$ as the first argument of the two-variable function $w_{\psi2}(x_1, x_2)$.

For any continuous one-to-one map $q = f(p)$ with a differentiable inverse $p = g(q)$, $C_\rho = g(C_\psi)$, and $\dot{\rho} = \dot{\psi} g'(C_\psi)$, with $g'(C_\psi) = dg(q)/dq|_{q=C_\psi}$, leading to

$$N_\rho^+(C_\rho, T) = \int_{t_0}^{t_0+T} dt \int_0^\infty \dot{\rho} w_{\rho2}(C_\rho, g'(C_\psi)) [g'(C_\psi)]^2 d\dot{\rho}. \quad (20)$$

With $w_{\rho2}(\rho, \dot{\rho})$ as defined by Eq. (15), the joint probability distribution of ψ and $\dot{\psi}$ is found via $w_{\psi2}(\psi, \dot{\psi}) = w_{\rho2}(g(\psi), g'(C_\psi)\dot{\psi}) [g'(C_\psi)]^2$. Plugging this expression into Eq. (19) gives

$$N_\psi^+(C_\psi, T) = \int_{t_0}^{t_0+T} dt \int_0^\infty \dot{\psi} w_{\rho2}[g(C_\psi), g'(C_\psi)\dot{\psi}] \times [g'(C_\psi)]^2 d\dot{\psi}. \quad (21)$$

Combining Eq. (21) with Eq. (6), we find

$$N_\psi^+(C_\psi, T) = N_\rho^+[g(C_\psi), T]. \quad (22)$$

Provided that $\eta(t)$ is stationary, Eqs. (6), (12), (21), and (22) yield

$$v_\psi(C_\psi) = T^{-1} N_\psi^+(C_\psi, T) = v_\rho[g(C_\psi)]. \quad (23)$$

In a specific case of MI-induced small-scale self-focusing, $\psi(t) = f([\rho(t)]) = I(t) = [\rho(t)]^2/2$, $f(\rho) = \rho^2/2$, $g(q) = (2q)^{1/2}$, $C_\psi = f(C_\rho) = C_\rho^2/2 = I_{\text{MI}}$, Eq. (23) becomes

$$v_I(I_{\text{MI}}) = v_\rho[g(I_{\text{MI}})] = v_\rho(2^{1/2} I_{\text{MI}}^{1/2}). \quad (24)$$

Combining Eqs. (16) and (24), we find

$$v_I(I_{\text{MI}}) = \varepsilon[(2I_{\text{MI}})^{1/2}/\sigma] \exp[-(a^2 + 2I_{\text{MI}}/\sigma^2)/2] \times I_0(a(2I_{\text{MI}})^{1/2}/\sigma). \quad (25)$$

Equation (25) expresses the count rate v_I as a function of the signal-to-noise ratio a and the dimensionless parameter I_{MI}/σ^2 . Our aim, however, is to understand the properties of v_I as a function of a and the ratio $x = I_{\text{MI}}/\bar{I}$ of the MI threshold I_{MI} to the mean intensity of the laser beam $\bar{I} = \langle \rho^2 \rangle / 2$ as a measure of how deeply subthreshold the self-focusing is. To isolate the dependence of v_I on $x = I_{\text{MI}}/\bar{I}$, we calculate $\bar{I} = \langle \rho^2 \rangle / 2$ via a statistical averaging of ρ^2 with a probability density function as defined by Eq. (6). The integral involved in this calculation is found as $\bar{I} = \langle \rho^2 \rangle / 2 = \mu_2/2$ from

$$\mu_k = \int_{-\infty}^\infty \rho^k W_\rho(\rho) d\rho = 2^{k/2} \sigma^k \Gamma(1 + k/2) L_{k/2}[-\rho_s^2/(2\sigma^2)], \quad (26)$$

where $\Gamma(n)$ is the gamma function and $L_\nu(x)$ is the Laguerre polynomial. Setting $k = 2$ in Eq. (26) for $\bar{I} = \langle \rho^2 \rangle / 2 = \mu_2/2$, we find $L_1[-\rho_s^2/(2\sigma^2)] = 1 + \rho_s^2/(2\sigma^2)$, leading to

$$\bar{I} = \sigma^2(1 + a^2/2). \quad (27)$$

Solving Eq. (27) for σ and plugging the solution into Eq. (25), we derive

$$v_I(I_{\text{MI}}) = v_I(x) = \varepsilon x^{1/2} (a^2 + 2)^{1/2} \exp\{-[a^2(x + 1) + 2x]/2\} I_0(ax^{1/2} (a^2 + 2)^{1/2}). \quad (28)$$

Equation (28) is one of the central results of our treatment. With $x > 1$, it provides a closed-form analytical solution for the count rate of subthreshold, $\bar{I} < I_{\text{MI}}$ self-focusing events in nonlinear beam dynamics of a noisy laser field. When $x < 1$, on the other hand, the mean intensity \bar{I} is above the I_{MI} threshold. For such \bar{I} , $v_I(I_{\text{MI}})$ is the count rate of downward crossings from the above-threshold region to the region below the I_{MI} threshold, where self-focusing does not occur

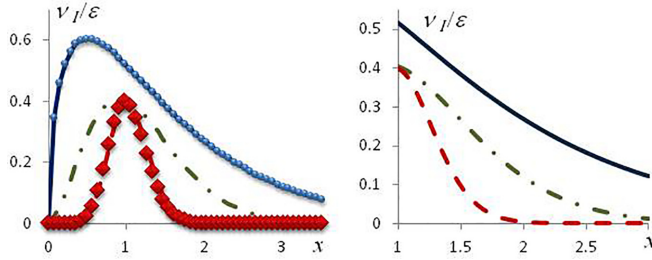


FIG. 3. (a) The normalized count rate v_I/ϵ calculated with (solid, dashed, and dash-dotted lines) Eq. (28), (diamonds) Eq. (29), and (circles) Eq. (32) as a function of $x = I_{\text{MI}}/\bar{I}$ for $a = 0.1$ (blue solid line), 3 (green dash-dotted line), and 8 (red dashed line). (b) The normalized count rate v_I/ϵ of subthreshold, $I_{\text{MI}}/\bar{I} \gg 1$ self-focusing events calculated with Eq. (28) for $a = 0.1$ (solid line), 3 (dash-dotted line), and 7 (dashed line).

[Figs. 2(c) and 2(d)]. In other words, with $x < 1$, $v_I(I_{\text{MI}})$ gives the count rate of events of no self-focusing. For very low x , the gap between \bar{I} and I_{MI} is very large, leading to a very small number of excursions to the subthreshold, $\bar{I} < I_{\text{MI}}$ region. In this regime, $v_I(I_{\text{MI}})$ becomes very low, tending to zero in the most general setting as $x \rightarrow 0$ [Fig. 3(a)], indicating that no-self-focusing events are extremely rare.

As one of the key properties of Eq. (28), the factor $\epsilon = [|R_0''| / (2\pi)]^{1/2}$ in this solution isolates effects of the noise bandwidth and the shape of the noise spectrum. Indeed, with $|R_0''|$ expressed, from Eq. (4), as $|R_0''| = (2\pi)^{-1} \int_{-\infty}^{\infty} \omega^2 S(\omega) d\omega$, $|R_0''|^{1/2}$ is recognized as a measure of the bandwidth of the noise component of the laser field (2). Accordingly, $\tau_c = 2\pi / |R_0''|^{1/2}$ provides a measure of the respective correlation time.

V. UNDERSTANDING THE ROLE OF THE SIGNAL-TO-NOISE RATIO

Equation (28) offers important insights into the role of the signal-to-noise ratio a as a parameter that controls the properties of the count rate $v_I(x)$ [Figs. 3(a) and 3(b)], defining how probable extreme subthreshold self-focusing events are. To understand the significance of a , we first examine the properties of $v_I(x)$ in the $a \gg 1$ limit, in which the driver $\eta(t)$ is dominated by the deterministic component, while the noise $\xi(t)$ is weak. In this limit, Eq. (28) reduces to

$$v_I(x) = \epsilon(2\pi)^{-1/2} \exp[-a^2(x^{1/2} - 1)^2/2]. \quad (29)$$

In Fig. 3(a), the plot of $v_I(x)$ calculated by using Eq. (29) (diamonds) is seen to closely follow the plot of $v_I(x)$ calculated with the exact result of Eq. (28) (red dashed line). The count rate $v_I(x)$ for $a \gg 1$ beams peaks at $x = 1$, which translates into $I_{\text{MI}} = \bar{I}$ on the field-intensity scale. As $x = I_{\text{MI}}/\bar{I}$ increases above $x > 1$, $v_I(x)$ rapidly falls off [dashed line and diamonds in Fig. 3(a)], displaying an exponential behavior in the $x \gg 1$ limit,

$$v_I(x) \approx \epsilon(2\pi)^{-1/2} \exp(-a^2 x/2). \quad (30)$$

Deeply subthreshold, $I_{\text{MI}}/\bar{I} \gg 1$ self-focusing of low-noise, $a \gg 1$ beams is thus a rare event whose count rate decays exponentially with I_{MI}/\bar{I} [red dashed line in Fig. 3(b)]. In the

case of a purely deterministic field, $a \rightarrow \infty$, the count rate $v_I(x)$ in Eq. (29) becomes a delta function, thus restoring the status of I_{MI} as a self-focusing threshold. In this regime, small-scale self-focusing is only possible for laser beams with $\bar{I} \geq I_{\text{MI}}$, in agreement with the canonical treatment of MI-induced self-focusing of deterministic laser beams.

As I_{MI} is set exactly at \bar{I} , the mean number of upward excursions that $I(t)$ makes across the MI threshold I_{MI} within the time interval $\tau_c = 2\pi / |R_0''|^{1/2}$ is

$$\mathcal{N}_I(I_{\text{MI}}) = \tau_c v_I(I_{\text{MI}} = \bar{I}) = 1 \quad (31)$$

This result is readily understood in terms of an intuitive physical picture. Indeed, with the threshold I_{MI} set exactly at \bar{I} , the field intensity $I(t) = [\rho(t)]^2/2$ of a purely deterministic driver, i.e., a driver with no noise component, $\xi(t) = 0$, would have made no excursions to the region above the threshold. A driver with a high, yet finite a , however, includes a weak, yet nonzero noise component, which gives rise to excursions of $I(t)$ above I_{MI} . When the threshold I_{MI} is set exactly at \bar{I} , each upward fluctuation imposed by the noise component of $\eta(t)$ translates into an excursion into the region above the threshold. Thus, within the correlation time $\tau_c = 2\pi / |R_0''|^{1/2}$, the mean number of above-threshold excursions is exactly one, exactly as Eq. (31) suggests.

In the opposite limit of a noisy field with a very low a , the behavior of $v_I(I_{\text{MI}})$ is drastically different. To appreciate this, we first consider the case of a field waveform with $a = 0$, i.e., a pure-noise waveform whose deterministic part is zero, $\rho_s = 0$. For such a waveform, the envelope distribution $W_\rho(\rho)$ [Eq. (6)] reduces to the Rayleigh probability density function, $W_\rho(\rho) = \mathcal{L}(v, 0) = \mathcal{R}(v)$. The count rate $v_I(x)$ is then given by

$$v_I(x) = \epsilon(2x)^{1/2} \exp(-x). \quad (32)$$

In Fig. 3(a), the plot of $v_I(x)$ calculated by using Eq. (32) (circles) is almost indistinguishable from the exact solution provided by Eq. (28) (blue solid line). The count rate $v_I(x)$ for $a \ll 1$ beams increases for small x , reaches its maximum, and then falls off with a further growth in x [solid line and circles in Fig. 3(a)]. Such a behavior of $v_I(x)$ reflects upon the properties of a field waveform with $a = 0$ as a random process with zero mean and intensity $\bar{I} = \sigma^2$. For such a waveform, $v_I(x)$ starts to fall off only when I_{MI} becomes much larger than $\bar{I} = \sigma^2$ [solid line and circles in Fig. 3(a)]. Unlike the count rate $v_I(x)$ for $a \gg 1$ beams, which falls off exponentially for $I_{\text{MI}}/\bar{I} \gg 1$ [Eq. (30)], the $I_{\text{MI}}/\bar{I} \gg 1$ behavior of $v_I(x)$ for $a \ll 1$ fields [Eq. (32)] is manifestly nonexponential [blue solid lines in Figs. 3(a) and 3(b)]. The heavy tail of $v_I(x)$ is indicative of a higher rate of $I_{\text{MI}}/\bar{I} \gg 1$ extreme self-focusing events for $a = 0$ fields compared to the rate of $I_{\text{MI}}/\bar{I} \gg 1$ self-focusing events for low-noise fields.

For field waveforms with intermediate signal-to-noise ratios, the behavior of $v_I(x)$ is intermediate between the distributions predicted by Eqs. (29) and (32) [dash-dotted lines in Figs. 3(a) and 3(b)], gradually evolving from the count rate as described by Eq. (32) toward $v_I(x)$ as expressed in Eq. (29) with a growth in the signal-to-noise ratio a .

VI. STOCHASTIC PROPERTIES OF A MULTIMODE LASER

Equations (28)–(32) provide a closed-form solution for the count rate of extreme self-focusing events universally applicable to a vast range of stochastic field-evolution scenarios in which the input field is a superposition [Eq. (2)] of a deterministic waveform and a narrowband, normally distributed stationary noise. To illustrate how fields of such a nature can emerge in a laser-experiment setting, we consider a generic laser source, whose output is a mixture of N modes,

$$y(t) = \sum_{n=1}^N b_n \cos(\omega_n t + \varphi_n) = \sum_{n=1}^N b_n \cos \Phi_n. \quad (33)$$

The characteristic function of such a process,

$$\theta(u) = \langle \exp(iyu) \rangle \quad (34)$$

is

$$\theta(u) = \prod_{n=1}^N \theta(ub_n), \quad (35)$$

where

$$\begin{aligned} \theta(ub_n) &= \langle \exp(iub_n \cos \Phi_n) \rangle \\ &= (2\pi)^{-1} \int_{-\pi}^{\pi} \exp[iub_n \cos(\omega_n t + \varphi_n)] d\varphi_n \\ &= J_0(ub_n) \end{aligned}$$

is the characteristic function of the n th mode, and $J_0(\zeta)$ is the zeroth-order Bessel function of ζ .

The distribution function of y is then found as

$$w(y) = (2\pi)^{-1} \int_{-\infty}^{\infty} \theta(u) \exp(-iuy) du, \quad (36)$$

leading to

$$w(y) = (2A)^{-1} \left[1 + 2 \sum_{k=1}^{\infty} \cos(\pi ky/A) \prod_{n=1}^N J_0(\pi k a_n/A) \right], \quad (37)$$

where $A = \sum_{n=1}^N a_n$.

For low N , the distribution $w(y)$ is distinctly non-Gaussian. It becomes Gaussian, however, as $N \rightarrow \infty$. To see this, we consider a process $z(t) = N^{-1/2}y(t)$. The characteristic function of such a process with $b_n = b$ is

$$\theta_z(u) = [J_0(N^{-1/2}bu)]^N. \quad (38)$$

In the $N \gg 1$ limit,

$$\ln[\theta_z(u)] \approx -(bu)^2/4 + (bu)^4/(64N), \quad (39)$$

leading to [33]

$$w(z) = (\pi)^{-1/2} b^{-1} [1 - (64N)^{-1} H_4(z/b)] \exp(-z^2/b^2), \quad (40)$$

where $H_n(x)$ is the n th-order Hermite polynomial.

As $N \rightarrow \infty$, both $w(z)$ and $w(y)$ become Gaussian, with

$$w(y) = (2\pi)^{-1/2} \sigma^{-1} \exp[-y^2/(2\sigma^2)], \quad (41)$$

$$2\sigma^2 = Nb^2.$$

We now see that, as the number of lasing modes N increases, the distribution of a multimode lasing process (33) converges to a Gaussian distribution regardless of the spectrum of the lasing modes $\{\omega_n\}$. The lowest-order moments of y are $\langle y^2 \rangle = Nb^2/2 = \sigma^2 = \bar{I}$, $\langle y^4 \rangle = 3[1 - (2N)^{-1}] \bar{I}^2$, $\langle y^6 \rangle = 15[1 - 3(2N)^{-1} + 2(3N^2)^{-1}] \bar{I}^3$. With $N \rightarrow \infty$, these moments recover the moments of a Gaussian random process [42].

Archetypes of laser sources capable of delivering stochastic field waveforms that can give rise to self-focusing, MIs, and laser-induced damage are found among high-power gas and solid-state lasers [43,44], as well as fiber lasers with a multimode- or multibeam-combining output [45,46]. An estimate on the correlation time $\tau_c = 2\pi/|R_0''|^{1/2}$, as one of the key parameters defining the count rate of stochastic self-focusing, is readily available for the latest generation high-energy excimer lasers, whose terahertz output bandwidths place τ_c at ≈ 1 ps [43,44]. For fiber lasers with incoherent beam combining, on the other hand, a typical beam-combining bandwidth $\delta\lambda \approx 10$ nm [45,46] at $\lambda \approx 1$ μm , suggests correlation-time estimates of the same order of magnitude, $\tau_c \approx \lambda^2/(c\delta\lambda) \approx 1$ ps.

With a standard estimate on the nonlinear refractive index of quartz glass taken at $n_2 \approx 2 \times 10^{-16}$ cm^2/W , a deterministic $\lambda \approx 1$ μm laser beam becomes unstable for $IL \geq 50$ GW/cm . Thus, with the field-intensity–path-length product set at $IL \approx 6.25$ GW/cm , a deterministic laser pulse with $\lambda \approx 1$ μm will be stable, with a comfortable margin of safety, against MI-driven beam breakup. However, a stochastic pulse with $a = 0$ and $\tau_c \approx 1$ ps with the same field intensity will give rise, in accordance with Eq. (32), to a $\nu_I \tau_p \approx 1$ self-focusing event per $\tau_p \approx 0.3$ ns laser pulse, thus dramatically increasing the risk of laser-induced damage.

VII. DISPERSION AND PULSE STRETCHING

Because of intracavity dispersion, the phase and group velocities of individual lasing modes in a multimode laser output, as well as their phases Φ_n are different. However, as long as the intracavity dispersion is deterministic, which is almost always the case for the existing solid-state and fiber-optic lasing settings, these dispersion-induced changes in phases Φ_n and the related slips of the carrier-envelope phase of the laser output have no effect on the statistics of the laser output and, therefore, cannot prevent the distribution $w(y)$ from universally converging to a Gaussian distribution in the $N \gg 1$ limit, as dictated by Eqs. (40) and (41). The closed-form solution for the count rate of extreme self-focusing events as provided by Eqs. (28)–(32) is thus invariant with respect to changes in intracavity dispersion, remaining applicable for a vast variety of multimode laser sources and a broad range of multimode field-evolution scenarios.

While an added deterministic dispersion has no effect on the distribution $w(y)$ and its convergence to a respective Gaussian distribution in the large- N limit [Eqs. (40) and (41)], it can lead to pulse stretching, thus lowering the peak power and the peak intensity of the laser beam. Because such dispersion-induced pulse stretching will decrease the mean intensity of the laser beam \bar{I} and inasmuch as it lowers \bar{I} the probability of self-focusing will be diminished. Such

self-focusing suppression via a dispersion-induced stretching of random field waveforms would represent an extension of the celebrated concept and technology of chirped-pulse amplification to stochastic field waveforms. Unlike the self-focusing of deterministic field waveforms, however, the self-focusing of stochastic beams is never totally avoided, but can only be suppressed in a statistical sense. Equations (28)–(32) provide a quantitative measure for the extent to which stochastic self-focusing can be suppressed as it yields the self-focusing count rates $\nu_I(x)$ as decreasing functions of $x = I_{\text{MI}}/\bar{I} > 1$, allowing the absolute values of $\nu_I(x)$ and their roll-off rates as functions of x to be defined, as shown in Figs. 3(a) and 3(b), for the specific bandwidth, intensity, and signal-to-noise ratio of the driver field waveform.

VIII. A BIGGER PICTURE

The analysis presented in this study is concerned with beam-stability thresholds in stochastic nonlinear optics, aiming to identify conditions under which stochastic beams become prone to self-focusing and MIs. While this study answers the question of *when* stochastic beams become unstable, it does not address the question of *how* such instabilities unfold. To answer this latter question, nonlinear spatiotemporal field-evolution equations need to be solved for a specific stochastic pulse envelope and a specific stochastic beam profile. The present study can be viewed as the first step of such an analysis.

The realm of closed-form solutions for the extreme-event count rates as provided by Eqs. (28)–(32) is in no way limited to optics, but extends, via the universal arguments behind these solutions, to a vast variety of processes that can be understood in terms of a nonlinear transform $f(\rho)$ of the envelope of a stochastic waveform (2). Specifically, nonexponential tails of $\nu_I(x)$ as predicted by Eqs. (28) and (32) are universal signatures of enhanced rare-event counts, often referred to as rogue waves [47,48], in a broad variety of settings

ranging from ocean waves [49] to optical soliton dynamics [50] and epileptic seizures [51]. Some of these rogue-wave settings, such as forest fires [52] or an emerging complexity of neuronal dynamics [53,54], are also a focus of studies concerned with self-organized criticality. The physical picture and mathematical framework in which such rare-event phenomena emerge in our study, however, does not invoke a critical state as an essential point in a stochastic field-waveform evolution. Thus, while the relation of solutions (28)–(32) to self-organized criticality is intriguing, self-organized criticality is not necessary for a system to reach solutions (28)–(32). These solutions are thus applicable to a broad class of processes beyond those exhibiting the self-organized criticality.

IX. CONCLUSION

To summarize, we derived a closed-form analytical solution for the count rate of extreme self-focusing events in nonlinear beam dynamics of noisy laser fields deeply below the self-focusing threshold. Analysis of this solution shows that the rare-event statistics of such deeply subthreshold self-focusing is highly sensitive to the signal-to-noise ratio and the bandwidth of the laser field waveform. For low-signal-to-noise beams, the rare-event distribution of deeply subthreshold self-focusing is shown to exhibit a manifestly nonexponential tail, thus indicating the enhancement of extreme self-focusing events. The subthreshold self-focusing is further enhanced by a broader bandwidth of the noise component of the laser field. It is such broadband, low-signal-to-noise laser fields that are especially prone to deeply subthreshold, rogue-wave self-focusing, lowering, via a laser-induced breakdown, the lifetime of downstream optics.

ACKNOWLEDGMENT

This research was supported in part by the Welch Foundation (Grant No. A-1801–20210327).

-
- [1] Y. R. Shen, *The Principles of Nonlinear Optics* (Wiley-Interscience, New York, 1984).
 - [2] S. A. Akhmanov, A. P. Sukhorukov, and R. V. Khokhlov, *Sov. Phys. Usp.* **10**, 609 (1968).
 - [3] *Self-Focusing: Past and Present*, edited by R. W. Boyd, S. G. Lukishova, and Y. Shen, Topics in Applied Physics, Vol. 114 (Springer, New York, 2009).
 - [4] E. Garmire, R. Y. Chiao, and C. H. Townes, *Phys. Rev. Lett.* **16**, 347 (1966).
 - [5] N. F. Pilipetsky and A. R. Rustamov, *JETP. Lett.* **2**, 55 (1965).
 - [6] D. E. Spence, P. N. Kean, and W. Sibbett, *Opt. Lett.* **16**, 42 (1991).
 - [7] H. A. Haus, *J. Sel. Top. Quantum Electron.* **6**, 1173 (2000).
 - [8] A. Couairon and A. Mysyrowicz, *Phys. Rep.* **441**, 47 (2007).
 - [9] L. Bergé, S. Skupin, R. Nuter, J. Kasparian, and J.-P. Wolf, *Rep. Prog. Phys.* **70**, 1633 (2007).
 - [10] A. M. Zheltikov, *J. Phys. B: At., Mol. Opt. Phys.* **50**, 09200 (2017).
 - [11] *The Supercontinuum Laser Source: The Ultimate White Light*, edited by R. Alfano (Springer, New York, 2022).
 - [12] A. Zheltikov, *J. Opt. Soc. Am. B* **36**, A168 (2019).
 - [13] A. V. Mitrofanov, D. A. Sidorov-Biryukov, M. M. Nazarov, A. A. Voronin, M. V. Rozhko, A. B. Fedotov, and A. M. Zheltikov, *Opt. Lett.* **46**, 1081 (2021).
 - [14] D. Strickland and G. Mourou, *Opt. Commun.* **55**, 447 (1985).
 - [15] M. D. Perry and G. Mourou, *Science* **264**, 917 (1994).
 - [16] G. Fibich and A. L. Gaeta, *Opt. Lett.* **25**, 335 (2000).
 - [17] R. W. Boyd, *Nonlinear Optics* (Academic, Boston, MA, 1992).
 - [18] V. I. Bespalov and V. I. Talanov, *JETP Lett.* **3**, 307 (1966).
 - [19] V. V. Shkunov and D. Z. Anderson, *Phys. Rev. Lett.* **81**, 2683 (1998).
 - [20] A. A. Voronin, A. M. Zheltikov, T. Ditmire, B. Rus, and G. Korn, *Opt. Commun.* **291**, 299 (2013).
 - [21] A. Zheltikov, *Opt. Express* **24**, 20716 (2016).
 - [22] E. A. Khazanov, S. Yu. Mironov, and G. Mourou, *Phys. Usp.* **62**, 1096 (2019).

- [23] A. A. Voronin and A. M. Zheltikov, *Phys. Rev. A* **94**, 023824 (2016).
- [24] V. Shumakova, P. Malevich, S. Ališauskas, A. Voronin, A. M. Zheltikov, D. Faccio, D. Kartashov, A. Baltuška, and A. Pugžlys, *Nat. Commun.* **7**, 12877 (2016).
- [25] P. A. Zhokhov, V. Ya. Panchenko, and A. M. Zheltikov, *Phys. Rev. A* **86**, 013835 (2012).
- [26] A. Voronin and A. Zheltikov, *Sci. Rep.* **7**, 36263 (2017).
- [27] M. Lenzner, J. Krüger, S. Sartania, Z. Cheng, Ch. Spielmann, G. Mourou, W. Kautek, and F. Krausz, *Phys. Rev. Lett.* **80**, 4076 (1998).
- [28] P. A. Zhokhov and A. M. Zheltikov, *Phys. Rev. Lett.* **113**, 133903 (2014).
- [29] A. M. Zheltikov, A. L'Huillier, and F. Krausz, in *Handbook of Lasers and Optics*, edited by F. Träger (Springer, New York, 2007), pp. 157–248.
- [30] T. Brabec and F. Krausz, *Rev. Mod. Phys.* **72**, 545 (2000).
- [31] P. A. Zhokhov and A. M. Zheltikov, *Phys. Rev. A* **96**, 033415 (2017).
- [32] S. M. Rytov, Yu. A. Kravtsov, and V. I. Tatarsky, *Introduction to Statistical Radiophysics, Part II: Random Fields* (Nauka, Moscow, 1978).
- [33] S. A. Akhmanov, Yu. E. D'yakov, and A. S. Chirkin, *Introduction to Statistical Radiophysics and Optics* (Nauka, Moscow, 1981).
- [34] S.O. Rice, *Bell System Tech. J.* **23**, 282 (1944).
- [35] S. O. Rice, *Bell System Tech. J.* **27**, 109 (1948).
- [36] P. I. Kuznetsov, R. L. Stratonovich, and V. I. Tikhonov, *Zh. Tekh. Fiz.* **24**, 103 (1954).
- [37] H. Steinberg, P. M. Schultheiss, C. A. Wogrin, and F. Zweig, *J. Appl. Phys.* **26**, 195 (1955).
- [38] V. I. Tikhonov, *Sov. Phys. Usp.* **5**, 594 (1963).
- [39] V. A. Ivanov, *Theory Probab. Appl.* **5**, 319 (1960).
- [40] M. R. Leadbetter, *Ann. Math. Statist.* **37**, 260 (1966).
- [41] G. L. Stuber, *Principles of Mobile Communication* (Kluwer, Boston, MA, 1996).
- [42] W. Bryc, *The Normal Distribution: Characterizations with Applications* (Springer, Berlin, 1995).
- [43] S. Obenschain, R. Lehmberg, D. Kehne, F. Hegeler, M. Wolford, J. Sethian, J. Weaver, and M. Karasik, *Appl. Opt.* **54**, F103 (2015).
- [44] E. M. Campbell, T. C. Sangster, V. N. Goncharov, J. D. Zuegel, S. F. B. Morse, C. Sorce, G. W. Collins, M. S. Wei, R. Betti, S. P. Regan, D. H. Froula, C. Dorrer, D. R. Harding, V. Gopalaswamy, J. P. Knauer, R. Shah, O. M. Mannion, J. A. Marozas, P. B. Radha, M. J. Rosenberg, T. J. B. Collins, A. R. Christopherson, A. A. Solodov, D. Cao, J. P. Palastro, R. K. Follett, and M. Farrell, *Philos. Trans. R. Soc. A* **379**, 0011 (2020).
- [45] T. Y. Fan, *IEEE J. Quantum Electron.* **11**, 567 (2005).
- [46] S. J. Augst, J. K. Ranka, T. Y. Fan, and A. Sanchez, *J. Opt. Soc. Am. B* **24**, 1707 (2007).
- [47] M. Onorato, S. Residori, U. Bortolozzo, A. Montina, and F. T. Arecchi, *Phys. Rep.* **528**, 47 (2013).
- [48] J. M. Dudley, G. Genty, A. Mussot, A. Chabchoub, and F. Dias, *Nat. Rev. Phys.* **1**, 675 (2019).
- [49] K. Dysthe, H. E. Krogstad, and P. Müller, *Annu. Rev. Fluid Mech.* **40**, 287 (2008).
- [50] J. M. Dudley, F. Dias, M. Erkintalo, and G. Genty, *Nat. Photonics* **8**, 755 (2014).
- [51] C. Witton, S. V. Sergeev, E. G. Turitsyna, P. L. Furlong, S. Seri, M. Brookes, and S. K. Turitsyn, *J. Neural Eng.* **16**, 056019 (2019).
- [52] B. D. Malamud, G. Morein, and D. L. Turcotte, *Science* **281**, 1840 (1998).
- [53] D. R. Chialvo, *Nat. Phys.* **6**, 744 (2010).
- [54] C. Bédard, H. Kröger, and A. Destexhe, *Phys. Rev. Lett.* **97**, 118102 (2006).